European Polymer Journal 186 (2023) 111836

Contents lists available at ScienceDirect

European Polymer Journal

journal homepage: www.elsevier.com/locate/europolj

Multifunctional low temperature-cured PVA/PVP/citric acid-based hydrogel forming microarray patches: Physicochemical characteristics and hydrophilic drug interaction

Achmad Himawan [a,b], Qonita Kurnia Anjani [a], Usanee Detamornrat [a], Lalitkumar K. Vora [a], Andi Dian Permana [b], Rand Ghanma [a], Yara Naser [a], Dina Rahmawanty [a,d], Christopher J. Scott [c], Ryan F. Donnelly [a,*]

[a] School of Pharmacy, Queen's University Belfast, Belfast BT9 7AF, United Kingdom
[b] Department of Pharmaceutical Science and Technology, Faculty of Pharmacy, Universitas Hasanuddin, Makassar 90245, Indonesia
[c] Patrick G Johnson Centre for Cancer Research, Queen's University Belfast, Belfast BT97BL, UK
[d] Department of Pharmacy, Faculty of Mathematics and Natural Science, Universitas Lambung Mangkurat, Makassar 90245, Indonesia

ARTICLE INFO

Keywords:
Polymeric microneedle
Hydrogel
Hydrophilic drugs
Drug delivery
Therapeutic drug monitoring

ABSTRACT

The characteristics of multifunctional polymeric hydrogel-forming microarray patches based on poly(vinyl alcohol)/poly(vinylpyrrolidone)/citric acid composite crosslinked at 80 °C were investigated. The swelling study showed that this composite possesses a higher swelling degree than the same polymer heated at 130 °C due to a lower crosslink density, which was then confirmed by FTIR examination. Solid-state studies revealed that lower-temperature crosslinking does not provide enough energy for the polymer to rearrange itself into a crystalline form. However, this composite polymer was shown to possess acceptable mechanical strength to insert/penetrate into the skin. The patch can function both as a means to sample model hydrophilic drugs from the skin and to deliver them when combined with a melt-type polyethylene glycol reservoir. The hydrophilic interaction between the hydrogel and drugs was investigated. A drug with a higher diffusion coefficient, modelled by theophylline (diffusion coefficient = 16.17×10^{-6} cm^2/s), can be delivered more efficiently than fluorescent sodium (diffusion coefficient = 2.32×10^{-6} cm^2/s) or cyanocobalamin (diffusion coefficient = 7.31×10^{-6} cm^2/s). This is mainly due to theophylline's high permeability (permeability coefficient = 7.40×10^{-5} cm/s) and weak ability to interact with the hydrogel (coefficient of partitioning = 1.3). These results indicated that the diffusion coefficient could be a useful predictive parameter to determine the delivery efficiency of the system. Furthermore, the results provide insight into how to select a suitable hydrogel for drug monitoring or delivery involving hydrophilic compounds based on the hydrophilic interaction between the polymer and the drug.

1. Introduction

Hydrogels are crosslinked 3D networks of insoluble polymers capable of retaining water within their structure [1]. Due to the high water content, a hydrogel can act as a medium for water-miscible solutes to diffuse [2]. Upon drying, a hydrogel material will form a xerogel that can reswell when water is reintroduced [3]. A dry hydrogel can also be developed through solid-state chemistry, where the formation of the crosslinked network is induced after the aqueous polymeric blend is dehydrated. This material can be considered a hydrogel-forming polymer, as it will swell into a hydrogel upon absorbing water from its surroundings [4].

In 2012, hydrogel-forming microarray patches (HF-MAPs) fabricated from hydrogel-forming materials were introduced [4,5]. Similar to any other MAP design, HF-MAPs consist of tiny protruding needle-like structures arranged in an array attached to a base [6]. The needles' length varies, typically being<1 mm [7,8]. In the dried state, HF-MAPs possess enough mechanical strength to pierce the skin surface, bypassing the protective stratum corneum barrier. Upon insertion, HF-MAPs swell quickly through extracellular fluid uptake from the underneath skin layers and form a continuous and unblockable hydrogel conduit [9]. HF-MAPs are a versatile technology extensively studied for minimally

* Corresponding author.
E-mail address: r.donnelly@qub.ac.uk (R.F. Donnelly).

https://doi.org/10.1016/j.eurpolymj.2023.111836
Received 28 October 2022; Received in revised form 9 January 2023; Accepted 11 January 2023
Available online 18 January 2023

invasive patient monitoring [10,11] and drug delivery platforms [12-14]. For the latter purpose, HF-MAPs are often combined with drug-containing reservoirs [5,13] or used alone when the drugs are loaded into the hydrogel [15]. HF-MAPs can be fabricated from a polymeric mixture [5,15-17], and one of the most studied composite materials is a combination of poly(vinyl alcohol)/PVA and poly(vinylpyrrolidone)/PVP [18-20].

PVA/PVP microneedles are often thermally processed at high temperatures to induce ester bond-mediated crosslinking between pristine hydroxyl groups from PVA and carboxyl groups from polycarboxylic acid [18]. CA contains three carboxylic acid groups, where the two terminal groups are often involved in crosslinking reactions. It is relatively biocompatible compared to other alternatives, such as glutaraldehyde, and is often considered a green crosslinker due to its biological and environmental safety [18,21,22]. Heat treatment at 130 °C has been used in many studies involving PVA/PVP/CA HF-MAPs formulations [13,18,19].

An attempt to modulate the performance of PVA/PVP/CA HF-MAPs can be made by tweaking the crosslinking density of the hydrogel, either by altering the formulation (e.g., amount of crosslinker), process parameters (e.g., crosslinking time) or both [18]. Although it seems simple, these changes may affect the critical characteristics of HF-MAPs, such as swelling behaviour, patch insertion, and drug-hydrogel interaction [1,2]. This is particularly important for HF-MAPs based on ionic hydrogels due to their possible interplay with hydrophilic molecules. This work aims to address the utilisation of low-temperature processing of PVPA/PVP/CA-based HF-MAPs for hydrophilic drug monitoring and drug delivery purposes. We chose three different drug molecules, theophylline, sodium fluorescein and cyanocobalamin, that possess varying physicochemical properties, such as molecular size, charge and pKa value.

Herein, we report, for the first time, the successful formation of HF-MAPs with a PVA/PVP/CA blend processed at 80 °C. The HF-MAPs possess comparable mechanical properties and superior permeability compared to a similar formulation. The formulations can be used as therapeutic drug monitoring or drug delivery platforms. The HF-MAP formulations demonstrate the ability to sample three different model drug molecules from *ex vivo* experiments, and a sufficient quantity of analyte can be recovered using a simple extraction method with a relatively safe water-based solvent. We also report the ability of HF-MAPs to deliver three different hydrophilic drugs across full-thickness skin when combined with melt-type drug-containing reservoirs. In addition, we suggest evidence of the relationship of hydrogel-drug interactions with the delivery efficiency of water-soluble drugs using PVA/PVP/CA HF-MAPs, which can be useful to screen drug candidates that can be delivered using this system.

2. Materials and methods

2.1. Chemicals

The chemicals used in this study were theophylline, fluorescein sodium, PVA 87–89 % hydrolysed MW 85.000–124.000, anhydrous citric acid, methanol for HPLC, acetonitrile for HPLC, triethylamine, and phosphate buffer saline (PBS) tablets (pH 7.4, ionic strength 0.01 M) were purchased from Sigma Aldrich, Dorset, UK. Cyanocobalamin was purchased from Alfa Aesar, Heysham, UK. Plasdone®/PVP K-29/32 was purchased from Ashland, Kidderminster, UK. Water for the formulation, buffer solution, and HPLC was obtained from an ELGA Purelab Flex 2® ultrapure water purification system purchased from Vivendi Water System Ltd., Bucks, UK. Full-thickness skin samples were excised from the stillborn piglets.

2.2. Hydrogel film preparation and characterisation

2.2.1. Hydrogel film preparation

Hydrogel thin films were prepared from an aqueous blend of polymer and crosslinking agent according to the composition reported in a previous study [18,19]. The details of the composition and the crosslinking conditions are given in Table 1. Aqueous blends containing 15 % PVA, 10 % PVP and 1.5 % CA were prepared from polymer stock solutions. The primary stock solution of 25 % w/w PVA was prepared by mixing PVA granules with deionized water. The PVA dispersion was then heated to 80 °C in an oven for 24 h with occasional stirring until a clear, viscous liquid was obtained. For PVP, a 40 % w/w stock solution was prepared by dispersing PVP powder into deionized water, allowing it to hydrate overnight, and then stirring until a homogenous solution was acquired. The PVA/PVP/CA blend was then prepared by weighing each primary stock solution. The required amount of citric acid was weighed and dissolved in PVP solution. Then, the PVA solution and the remaining water were added and stirred into this mixture. The polymeric-acid blend was then centrifuged at 5000 rpm for 15 min to remove entrapped air bubbles.

To prepare the films, 150 µL of polymer and citric acid blend was pipetted into a silicone mould with a flat square template (12 × 12 × 3.2 mm) using a positive displacement micropipette. The solution was centrifuged at 5000 rpm for 10 min to form a polymer layer inside the mould. The mixture was air-dried at ambient temperature for 48 h. After drying, the thin film was collected and subjected to heating at 80 °C for 24, 48 and 72 h (for HF80-1, HF80-2 and HF80-3 formulations) and 130 °C for three hours (for HF130 formulation). Uncrosslinked hydrogels were labelled as HF0.

2.2.2. Swelling kinetics, porosity and surface pH

A swelling kinetics study was conducted using hydrogel films cut into approximately 0.5 × 0.5 cm pieces. The films were individually weighed, and the mass was then noted as m_0. Approximately 15 ml of PBS pH 7.4 was pipetted into a container where the thin films were immersed individually. The mass of the swollen hydrogel was then taken at determined time points by removing the film from the PBSS, lightly dabbed with filter paper and weighed carefully (m_t). After 48 h, the data for the final time point were taken and noted as m_∞. The swelling percentage was calculated using Equation (1), and a plot of %S vs t was drawn. The procedure was carried out at ambient temperature.

$$\%S = \left(\frac{m_t - m_0}{m_0}\right) \times 100 \quad (1)$$

The fully swollen hydrogel was then redried in an 80 °C oven overnight. The mass of the xerogel was weighted and noted as m_x. The equilibrium water content (EWC_{PBS}) and gel fraction (GF_{PBS}) were calculated using Equations (2) and (3), respectively.

$$EWC_{PBS}\,(\%) = \left(\frac{m_\infty - m_x}{m_x}\right) \times 100\% \quad (2)$$

$$GF_{PBS}\,(\%) = \frac{m_x}{m_0} \times 100\% \quad (3)$$

Table 1
Formulation composition and crosslinking condition.

	HF0	HF80-1	HF80-2	HF80-3	HF130
Composition					
PVA 85-124k	15 %	15 %	15 %	15 %	15 %
PVP K29/32	10 %	10 %	10 %	10 %	10 %
Citric Acid, Anhydrous	1.5 %	1.5 %	1.5 %	1.5 %	1.5 %
Water	73.5 %	73.5 %	73.5 %	73.5 %	73.5 %
Thermal Treatment					
Annealing Temp.	Untreated	80 °C	80 °C	80 °C	130 °C
Annealing Time	NA	24 h	48 h	78 h	3 h

To perform a morphology study, swollen film samples were first subjected to a freeze-drying cycle for 25 h (Table S1). The lyophilized hydrogels were carefully cut into halves, and the surface and cross-sectional morphology were observed with a Hitachi TM3030® Benchtop Scanning Electron Microscope (Hitachi Technology UK, Maidenhead, UK). The buffer solution pH used for the swelling study was also monitored at 1-hour and 24-hour intervals using a Hanna Instruments pH 209® digital pH meter (Hanna Instruments, Yorkshire, UK). These pH values were addressed as the estimated surface pH of the hydrogel.

The experimental data from the swelling curve were then fitted into Equation (4) to analyse its swelling behaviour.

$$\frac{t}{S} = A + Bt \tag{4}$$

In this equation, S is the mass ratio between water and imbibed water and the initial mass of the dried hydrogel (m_t-m_0/m_0), A is the reciprocal of the initial swelling rate ($1/k_s S_\infty^2$), and B is the inverse of equilibrium swelling ($1/S_\infty$). A graph of t/S vs t was drawn, and the extensive swelling parameters were derived from the best fit line.

The porosity of the dried hydrogels was evaluated using the organic solvent displacement method. In this experiment, ethanol was chosen as the solvent with a soaking time of 4 h. During this time, ethanol will be absorbed into the hydrogel without causing any swelling. The porosity values were calculated based on the weight difference before and after ethanol soaking using Equation (5).

$$Porosity = \frac{(m_{et} - m_0)}{V\rho} \tag{5}$$

where m_{et} is the mass of the hydrogel after being soaked in ethanol, m_0 is the initial mass of the hydrogel, V is the volume of dried hydrogel, and ρ is the density of ethanol [23].

2.2.3. Physicochemical characteristics of hydrogel films

In this study, we examine the physicochemical characteristics of hydrogel films using attenuated total reflection-Fourier transform infrared (ATR-FTIR) spectrometry, differential scanning calorimetry (DSC), thermogravimetric analysis (TGA), X-ray diffractometry (XRD) and Ultraviolet–visible(UV–vis) spectrophotometry. These techniques were used to elucidate various hydrogel properties before and after the crosslinking process.

All samples were subjected to ATR-FTIR analysis to study the hydrogel crosslinking process and chemical shift. A PerkinElmer Spectrum Two® FTIR Spectrometer (PerkinElmer, Buckinghamshire, UK) with Pike MIRacle® ATR attachment (Pike Technologies, Wisconsin, USA) was used to measure the absorbance of the materials in the infrared region. The individual sample was fitted into the ATR diamond head and secured using the instrument's screw mechanism. All hydrogel samples and starting materials' absorbance between wavenumbers of 4000 to 750 cm^{-1} was recorded at 4 cm^{-1} resolution. The results of an average of 128 scans were corrected against the background, and then the normalised values were plotted into graphs.

Differential scanning calorimetry (DSC), in conjunction with thermogravimetric analysis (TGA), was used to study the thermal properties of the hydrogels and their composition. Samples (5 to 10 mg) were weighed and placed inside a sealed aluminium crucible for DSC analysis. The TA Instrument DSC Q20® (TA Instruments, New Castle, Delaware, USA) was run in ramp mode with a heating rate of 10 °C/minute under nitrogen flow with a scanning range from 50 to 400 °C. For the TGA experiment, 5 to 10 mg of samples were placed inside an open aluminium crucible and fixed onto the automatic loader of the TA Instrument TGA Q50® system (TA Instruments, New Castle, Delaware, USA). The samples were heated in ramp mode with a heating rate of 10 °C/minute under nitrogen flow, and the weight change over time was recorded. A normalised plot of each thermogram was created, and important thermal events were tabulated.

A MiniFlex II Desktop Powder X-ray Diffractometer® (Rigaku Corporation, Kent, UK) equipped with Cu Kβ radiation operated at a voltage of 30 kV and a current of 15 was used to study the solid-state properties of the dried hydrogel alongside the raw ingredients. Each sample was placed into a sample holder with a 0.2 mm depression. All samples were scanned at a rate of 2.0°/min with an angular range of 10-60° 2θ. The XRD signal was processed with OriginPro 9® (OriginLab Corporation, Northampton, Massachusetts, USA), and the normalised intensity was plotted against 2θ for the final diffractogram.

The qualitative extractable study was performed in double-beam mode using an Agilent Cary 60® UV–vis spectrophotometer (Agilent Technologies UK Ltd, Stockport, UK). Approximately 10 ml of solvents (PBSS pH 7.4, methanol and acetonitrile) were individually placed into clear vials, where a piece of hydrogel was then submerged into the solvents. The vials were appropriately capped and put into a shaking incubator set at 37 °C, agitating at 40 rpm. The extraction process was carried out for 24 h. After that, the hydrogels were removed, and the extract was filtered before being placed inside a quartz cuvette. The spectra of the samples were then recorded from 400 to 800 nm with the corresponding solvent used as the blank.

2.3. In vitro permeation, partitioning, and drug extraction study

The in vitro studies were conducted using three different model molecules, namely, theophylline (THEO), cyanocobalamin (CYAN) and fluorescein sodium (FLUO). The three molecules chosen in this study have different molecular sizes, solubilities and physiological charges (the details are given in Table S2). These model molecules have been used to assess the permeability of PMVE/MAH-based hydrogels by our group in a previous study [2].

2.3.1. Analytical conditions

Two HPLC methods and one spectrophotometric method were developed for the purpose of this study. First, all analytes were subjected to a wavelength scan to confirm their maximum wavelength absorption (λ_{max}) in the UV–visible range. To perform this procedure, the analytes (THEO, CYAN and FLUO) were dissolved separately in PBSS pH 7.4 and diluted to 10 μg/mL and 1 μg/mL. Each analyte solution was pipetted into a 1 cm^3 quartz cell and scanned from 200 to 800 nm using an Agilent Cary 60® UV–Vis spectrophotometer in double-beam mode. PBSS was used for baseline correction, and the measurement was conducted at ambient temperature.

An Agilent 1220 Infinity® HPLC system with a UV lamp detector was used in method development and validation for THEO detection and quantification at its λ_{max}. Isocratic reversed-phase (RP) liquid chromatography was carried out on an X-Select® C18 column (150 mm × 4.6 mm, 5 μm particle size) maintained at 25 °C. The mobile phase was 0.1 % v/v TEA in water (pH 4.5) and MeOH (55:45) running at 1 m/min. The mobile phase was subjected to vacuum filtration using a 0.22 μm membrane filter before use. The chromatogram acquired from the system was analysed using Agilent OpenLAB CDS Chemstation® software. The same HPLC system and column were used for CYAN detection and quantification. For CYAN, the mobile phase consisted of 0.1 % v/v TEA in water (pH 7.0) and MeOH (65:35) running at 1 ml/min. The mobile phase was subjected to vacuum filtration using a 0.22 μm membrane filter before use.

A Fluostar OMEGA® microplate reader system was used to develop and validate a suitable spectrophotometric method for FLUO detection and quantification at its λ_{max}. An aliquot of 200 μL of sample was placed inside the well and measured in absorbance mode (for higher range) and fluorescence mode (for lower range) against the solvent as the blank. The spectral data acquired from the system were analysed using OMEGA® data analysis software.

2.3.2. In vitro permeation and partitioning studies

The hydrogels were tested for their permeability in Side-Bi-Side® horizontal diffusion cells. Before the test, the hydrogels were hydrated

by immersing them in PBSS pH 7.4 to equilibrium prior to the experiment. Each swollen hydrogel was fixed between the donor and acceptor compartments of the diffusion cell. The assembly was connected to a circulatory water bath maintained at 37 °C and secured on the magnetic stirring station, providing constant agitation at 600 rpm. The donor compartments were filled with 3 ml of analyte solution (THEO, CYAN or FLUO) in PBSS pH 7.4 with 1000 μg/mL concentration, whereas the acceptor compartments were filled with 3 ml of PBSS pH 7.4. The acceptor compartments were sampled at a defined time interval by completely draining all 3 ml of PBSS and immediately replacing it with a fresh buffer with the same volume. The samples were then analysed using the methods described in the analytical section.

The solute permeability coefficient, P, was calculated for each model molecule used by fitting the experimental data to the following equation:

$$\ln\left(1-\frac{2C_t}{C_0}\right) = -\frac{2A}{V}Pt \tag{6}$$

where C_t is the cumulative solute concentration in the receptor compartment at time t, and C_0 is the initial concentration in the donor. V is the volume of the liquid inside the cell, and A is the effective area of permeation. The value of P was obtained from the slope of the linear portion of a plot between $-(V/2A)*\ln(1-2C_t/C_0)$ versus t [2,24,25].

The diffusion coefficient, D, was calculated using the following equation:

$$D = \frac{PL}{K_d} \tag{7}$$

where L is the membrane thickness in the swollen state and K_d is the solute partition coefficient that was derived using Equation (8) as follows:

$$K_d = \frac{C_m}{C_s} = \left(\frac{C_0}{C_s}-1\right)\frac{V_0}{V_m} \tag{8}$$

K_d was determined experimentally through a drug equilibrium uptake study. In brief, a piece of fully swollen hydrogel was submerged in a drug solution with a concentration of 1000 μg/mL (C_0) for 24 h. Then, the concentration of the analyte in the solution was measured again (C_s).

2.3.3. Drug extraction and uptake

Aqueous solutions of each drug were prepared at 25, 100 and 250 μg/mL concentrations. Each solution was placed in separate glass vials, where a piece of dried hydrogel film weighing approximately 20–25 mg was subsequently submerged. The vials containing samples and control solution without hydrogel were placed in a shaking incubator at 37 °C and rotated at 40 rpm. After 20 min, the hydrogel was removed, patted dry with a piece of filter paper and placed into a clean vial. To the new vials, 1 ml of PBSS pH 7.4 was added, and the vials containing buffer solution and hydrogel were lightly shaken for 2 min to extract the analyte. Then, the solution was drawn, and the concentration of analyte in the extraction solution was measured according to the analytical method described in the analytical section. The quantity of analytes in the remaining stock solution (m_x) and control solution (m_0) were also measured using the same analytical method. The differences between m_0 and m_x were stated as the amount of analyte uptake by the hydrogels.

2.4. Microneedle array patch fabrication and characterisation

2.4.1. Microneedle array patch microfabrication

The hydrogel-forming microneedle array patches (HF-MAPs) were prepared from an aqueous blend of polymer and crosslinking agent according to the composition and steps described in the previous section. The selected hydrogel formulations were cast into 14 × 14 laser-engraved needle templates (pyramidal shape, 600 μm height, 450 μm base width and 350 μm interspacing) secured in a PDMS housing. The moulds were individually filled with 150 μL polymeric mixture, followed by centrifugation at 5000 rpm for 15 min and air-drying for 48 h at ambient temperature. After the polymer inside the moulds was dried (HF0), they were removed and crosslinked at 80 °C for 24 h (HF80-1) and 130 °C for 3 h (HF130).

2.4.2. MAP geometry and morphology

MAP samples were observed using a Leica EZ4 W® Stereo Microscope (Leica Microsystem Ltd, Milton Keynes, UK) at the appropriate optical magnification. Images of each array on all four sides were taken with the integrated camera in calibrated mode. The needle heights from three patches were measured using Leica Application Suite EZ® software. For morphology observation, the MAPs were placed on the Hitachi TM3030® Benchtop SEM platform using carbon adhesive discs. The needle image was taken at 100x magnification in topological mode.

2.4.3. MAPs physicomechanical properties

A height reduction test was performed to gauge the mechanical strength of the MAPs. The array was pressed against a solid and flat aluminium surface needle tip down using Stable Micro Systems TA.XT. Plus® Texture Analyser assembly (Stable Microsystem Ltd, Surrey, UK) at 0.053 N/needle and 0.163 N/needle (constant force mode) for 30 s. The needle height reduction was calculated based on the needle length before and after the test, measured with an optical stereo microscope [26].

The Parafilm-M® test was used to assess the insertion of the needle through membranes [27]. Eight layers of Parafilm-M® were stacked and placed on the Stable Micro Systems TA.XT. Plus® Texture Analyser platform. A piece of HF-MAP was then put needle side down (facing the film layers). The MAPs were then pressed against the membrane by the probe attached to the texture analyser at 32 N. This 32 N force was based on a previous study that measured the mean thumb pressure of human volunteers [27]. After the test, the layers were separated and individually observed under a light microscope. The holes created by the needles in each layer were counted. A graph of insertion depth vs percentage of the needle passing through the Parafilm-M® layer was created, where each layer of Parafilm-M® corresponded to an insertion depth of 130 μm.

An *ex vivo* skin insertion test was carried out using excised neonatal piglet skin to simulate its insertion into human skin. The full-thickness skin pieces were dehaired using hair removal cream and stored at −20 °C when not in use. Before the test, the skin was thawed under running water, soaked in PBS pH 7.4 for at least 20 min, dabbed dry, stretched and glued onto a solid surface. The HF-MAPs were applied using a thumb force and further secured with a piece of Tegaderm® dressing. The patch insertion was observed using Michelson Diagnostics EX1303® Optical Coherence Tomography connected to Santec HSL-2000® High-Speed Scanning Laser as the light source (Michelson Diagnostic Ltd, Kent, UK). The images were taken using National Instruments LabVIEW™ 8.5 and processed using Fiji ImageJ® software.

2.5. Ex vivo drug monitoring test

The capability of HF-MAPs in analyte uptake was evaluated using a modified Saarbrücken model [28]. Four layers of filter papers were stacked and placed into a petri dish. A piece of full-thickness neonatal porcine skin was then carefully placed on the surface of the filter paper. Subsequently, 7 ml of drug solution in PBSS pH 7.4 was added carefully from the side of the filter papers. The assembly was then covered with the lids and placed inside an oven set at 37 °C for 3.5 h. The excess liquid was removed carefully, and the skin surface was dabbed dry with tissue paper. A piece of skin was cut as a sample and placed into an Amicon® centrifugation tube filter (molecular weight cut-off of 10.000 kDa). The ISF from the skin was then separated from the tissue by spinning the samples in a centrifuge running at 14,000 rpm for 30 min. The liquid collected in the lower compartment of the tube was collected for

analysis.

For the drug monitoring study, the HF-MAPs were inserted into the preincubated skin using a thumb at a force of approximately 32 N/array for 30 s and secured in place with a 16 g metal weight (see Fig. 1). After one hour, the HF-MAPs were removed, placed in a 5 ml glass vial containing 1 ml of PBS pH 7.4, and lightly shaken for 2 min. The extraction solution was then collected in a 1.5 ml centrifuge tube. All ISF and extraction samples were subjected to quantitative analysis according to each drug analytical method.

2.6. Ex vivo drug delivery study

2.6.1. Melt-type reservoir formulation and characterisation

Drug powders (THEO, FLUO and CYAN) were formulated separately into melt-type PEG reservoirs using a melt moulding method. The PEG base for the reservoirs was made from a mixture of PEG 1000 and PEG 400 in a 9:1 ratio to achieve a melting point lower than 32 °C, the temperature at the skin's surface. In brief, the preweighed PEG base mixture was melted in a glass vial in an oven set at 37 °C. Drug powder was then mixed into the melted base in a 9:1 ratio, making the theoretical drug loading approximately 10 % of the total mixture. An aliquot (200 mg) of the PEG reservoir mixture was cast into a prewarmed silicone template (1 × 1 × 0.2 cm), spread evenly and placed at −20 °C to allow rapid cooling. The reservoirs were kept in the refrigerator until further use.

Each formulation was subjected to characterisation, including visual appearance, ATR-FTIR, melting time and DSC analysis. ATR-FTIR and DSC analyses were performed according to the method mentioned before in the hydrogel section. The melting time analysis was performed by placing the reservoir on the surface of preswollen hydrogel heated on top of an agarose layer that was cast inside a glass petri dish. A hotplate was used as a heat source to maintain the hydrogel temperature at 35 °C. The time taken for the PEG reservoir to completely melt was recorded using a digital stopwatch.

2.6.2. Franz cell experiment

The *ex vivo* drug delivery study through PVA/PVP/CA HF-MAPs in tandem with a melt-type reservoir for all three model drugs (THEO, FLUO and CYAN) across full-thickness skin was investigated. A modified Franz diffusion setup, as previously described, was used. Briefly, full-thickness neonatal porcine skin was carefully fixed to the donor compartment of the Franz diffusion cell (FDC-400 flat flange, 15 mm orifice) using cyanoacrylate glue with the SC facing upwards. HF-MAPs were inserted into the skin using a syringe plunger and manual force for 30 s. Following insertion, a melt-type PEG reservoir was placed on top of the HF-MAP. A cylindrical stainless steel weight (diameter 11 mm, weight 5 g) was placed on top of the assembly to prevent expulsion of the hydrogel-forming MN array from the skin. The donor compartment of the apparatus was placed onto the receiver compartment, clamped and sealed with Parafilm M to prevent unnecessary evaporation. An illustration of the assembly is given in Fig. 1B.

PBS pH 7.4 was used as the medium in the receptor compartment for the delivery study for all formulations. The receiver compartment buffer was degassed before use, stirred at 600 rpm and maintained at 37 ± 1 °C. A micropipette with tip extension was used to sample 200 μL of the receiver media at predetermined time intervals (0.5, 1, 2, 4, 8, 24 h), and the same volume of PBSS was later added to replace this aliquot. All samples were subjected to quantitative analysis according to their respective analytical methods. A graph of the amount of released drug vs time was constructed, and the data were analysed to determine its delivery kinetics.

2.6.3. Drug deposition study

To evaluate the residual drug residing in skin and hydrogel, skin samples and HF-MAP samples from the *ex vivo* drug delivery study were further processed. All skin samples were rinsed with PBS pH 7.4 and cut into smaller pieces (approximately < 0.2 cm in diameter) before placing them into 2 ml centrifuge tubes. Into the tubes, two pieces of stainless steel spheres (diam. 5 mm) and 500 μL of PBS pH 7.4 were placed. The tubes were then disrupted using a TissueLyser LT (Qiagen, Germantown, Maryland, USA) running at 50 rpm for 15 min. After that, the liquid was transferred into a different 1.5 ml centrifuge tube and centrifuged at 14,000 rpm for 15 min to separate any remaining solids from the supernatant. The supernatant was pipetted into a different tube, diluted accordingly and analysed using the appropriate method.

2.7. Graphing and statistical analysis

Graphing and processing of spectral, thermal and diffraction data were carried out using Origin Pro® version 9 (OrigibLab Corporation, Northampton, Massachusetts, USA). All data are presented as the means ± standard deviations (SD), and the number of replicates is indicated in the corresponding graph. Statistical analysis was performed using GraphPad Prism® version 9.3.1 (GraphPad Software, San Diego,

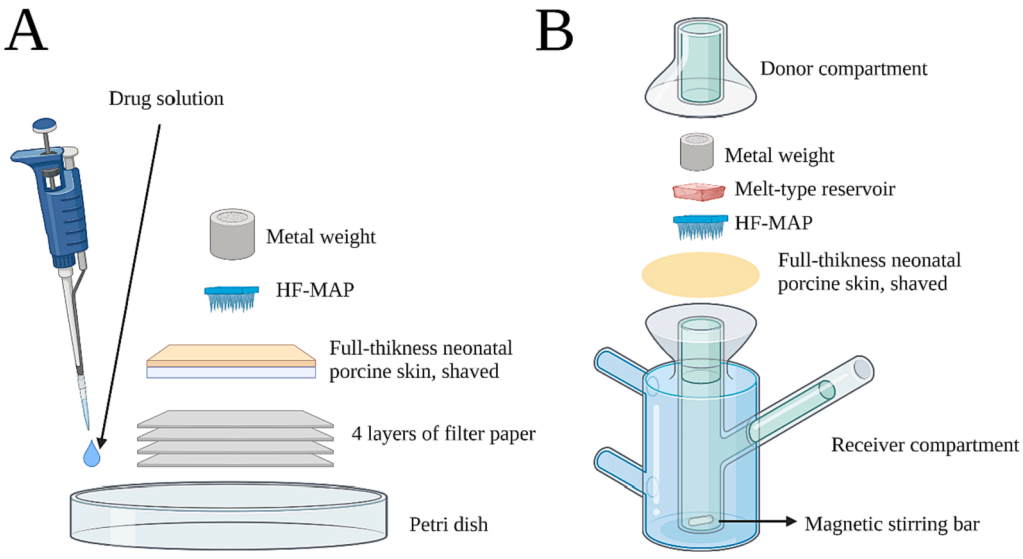

Fig. 1. (A) Set up for the modified Saarbrücken model for analyte uptake. MAPs and metal weight were placed after the preincubation period. (B) Illustration of the modified Franz diffusion cell (vertical diffusion cell) assembly for the *ex vivo* delivery study.

California, USA). All data were tested for normality with Shapiro–Wilk normality testing, and normally distributed data were subjected to ANOVA. Tukey's or Šídák's multiple comparison tests were used to compare the dataset. Nonnormal data were analysed using Kruskal–Wallis's test. The drug delivery kinetic models were evaluated using the MS Excel® DDsolver plugin [29].

3. Results and discussion

Four different hydrogel film formulations were successfully fabricated. The thin films heated at 130 °C appeared yellowish, while the other films treated at 80 °C underwent no appearance change other than becoming slightly opaque. It has been reported that the optimum temperature for crosslinking PVA/PVP/CA microneedles is 130 °C [18], but interestingly, other research has shown that temperatures as low as 50 °C could crosslink different types of PVA composite polymers for wound dressing applications [30].

In the composite polymer mixture, CA acts as a crosslinker between PVA macromolecule strands. The hydroxyl groups in the PVA chains will react with the terminal carboxylic group in CA, forming a new ester bond *via* the condensation route. This provides the new crosslinked polymer with a free carboxylic acid group available for ionisation [31]. There are three possible positions where CA could attach to the polymeric chain. The first position is where two terminal carboxylic groups form two ester bonds with different polymer chains, connecting those strands (A position). The second is when both terminal carboxylic acids form ester bonds with two different hydroxyl groups in the same PVA chain (B position), and the last is when only one terminal carboxylic group forms an ester bond and the other end is left unreacted (C position) [21,32,33]. On the other hand, PVP participates through the interaction of oxygen in the pyrrolidone ring and PVA hydroxyl groups, forming hydrogen bonds. This interaction is weaker than that of covalently bonded CA and PVA. A proposed reaction mechanism based on the information available in the literature is given in Fig. 2.

3.1. Swelling kinetics, porosity and surface pH

A swelling kinetics study was performed to assess the degree of swelling of each formulation. Swelling is an important characteristic of a hydrogel system because it determines the extent of its application. Highly swellable hydrogels can facilitate better permeation that might be preferred for drug delivery purposes [2]. The results in Fig. 3A-3B demonstrate that different crosslinking temperatures affect the swelling properties of the hydrogel. The formulation heated at 80 °C (HF80) swelled more than the formulation heated at 130 °C (HF130), even though the heating time at a lower temperature was substantially longer. It was observed that there was no significant difference ($p > 0.1$) in EWC_{PBS} and GF_{PBS} values between HF80-1, HF80-2 and HF80-3, but all values were significant when each HF80 formulation was compared to HF130 ($p < 0.0001$ for EWC_{PBS} and $p < 0.005$ for GF_{PBS}) (Table S3). An inverse relationship was observed between the EWC_{PBS} and GF_{PBS} values. Formulations with high EWC will have lower GF and *vice versa* [18]. The gel fraction reflects the portion of the composite hydrogel leached into the swelling media because the polymeric chain is not covalently linked to the hydrogel network [34]. We decided that we would only consider HF80-1 and HF130 for the rest of the study.

After 48 h, the hydrated hydrogels were subjected to a freeze-drying process to remove water from the polymer. The cross-sections of the xerogel were observed using SEM, and the results are given in Fig. 3C. It was clear that both hydrogels had distinct surface and cross-section appearances. HF80-1 appeared "sponge-like" with a porous surface, and HF130 had a scalier/crumbling appearance. Based on these results, it seems that the different temperatures during the crosslinking process triggered different conformations in the polymeric network of the composite hydrogel.

We further observed the change in pH of the swelling media. The results revealed that the pH of the buffer dropped as the swelling took place. The PBS solution pH dropped approximately 0.8 for HF80-1 and 0.4 for HF130 on a pH scale after 1 h of swelling. The pH decreased more after 24 h, approximately 1.8 and 1.2 on the pH scale for HF80-1 and HF130, respectively (Fig. 3D). The pH drop can be attributed to (1) a free carboxylic acid moiety from crosslinked CA and (2) unreacted CA molecules that were released to the swelling media [31]. Leaching of unreacted acid has been reported in another study where oxalic acid was used to crosslink PVA [35].

The hydrogel porosity gives insight into the density of the polymeric matrix. Its intrinsic porosity comes from the fact that a crosslinked polymer forms a mesh with a certain mesh size [36]. In this study, we tried to estimate the hydrogel intrinsic porosity in its dry state. The measurement results revealed that HF80-1 was less dense than HF130 (Table S1). PVA/PVP composites crosslinked with glutaraldehyde have been reported to have some degree of porosity [20].

3.2. Physicochemical characteristics of hydrogel films

FTIR analysis was performed to determine the chemical shift of the

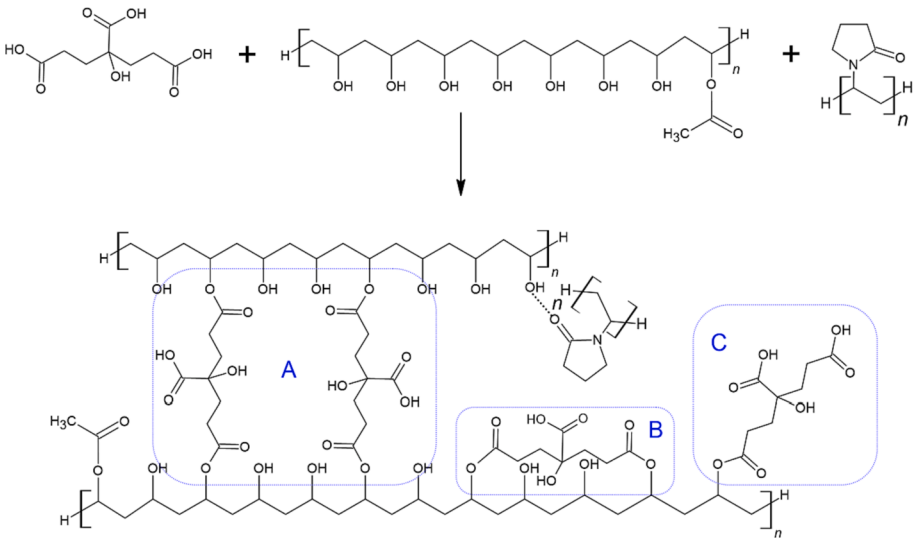

Fig. 2. Proposed crosslinking reaction mechanism speculating the position of citric acid after thermal treatment and how PVP interacts with the rest of the polymer.

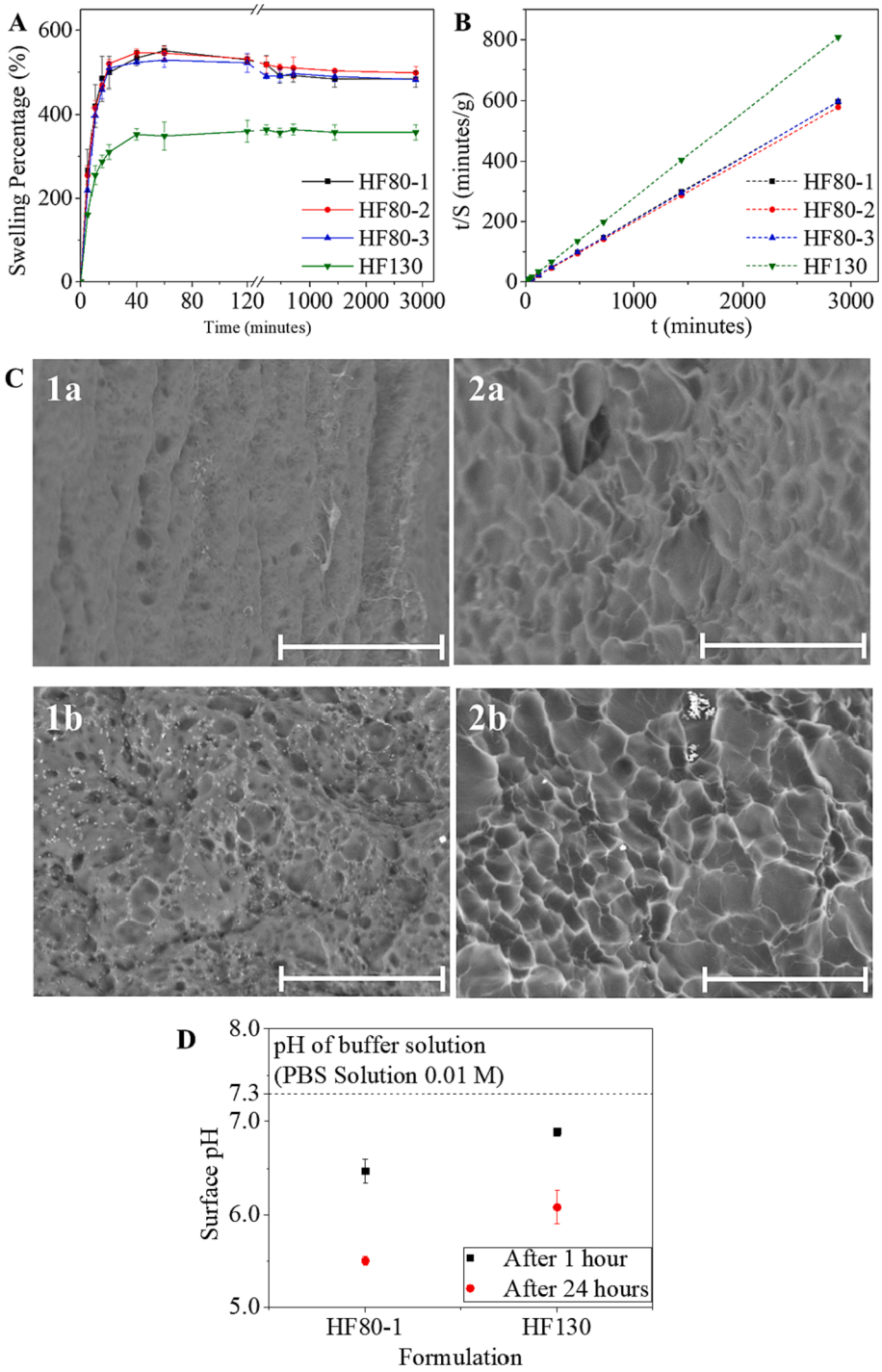

Fig. 3. Illustration of (A) swelling curve of the HF formulations in phosphate buffer saline solution; (B) curve t/S vs t of HF formulation in 0.01 M phosphate buffer saline (PBS) solution pH 7.4; (C) SEM images of swollen hydrogel surface (1a: HF80-1, 1b: HF130) and cross-section (2a: HF80-1, 2b: HF130) after freeze-drying (scale bar = 40 μm); (D) the graph of surface pH measurement.

polymer after crosslinking. The complete IR spectra of the hydrogels and their composition are given in Fig. 4A, and modes of interest are highlighted in Table S4. Pure PVA showed a broad O—H stretching band at ~ 3330 cm^{-1}, a split peak at ~ 2920 cm^{-1} corresponding to alkyl C—H stretching for both symmetrical and asymmetrical stretching, and characteristic C═O stretching peaks at ~ 1713 and 1732 cm^{-1} from the residual carbonyl ester side group [37]. PVP showed a strong peak at ~ 1655 cm^{-1}, attributed to NC═O stretching in its pyrrolidone rings. The band at ~ 1500 cm^{-1} was assigned to its characteristic C—N bond [38,39]. The sharp and low intensity peaks at ~ 3450 and ~ 3285 cm^{-1} corresponding to the O—H stretch in CA and the two C═O stretching modes at ~ 1695 and ~ 1745 cm^{-1} were assigned to the carboxylic group in the anhydrous citric acid dimer structure [40]. By further analysing the FTIR results, the formation of the crosslinked polymer was confirmed by comparing the ratio between hydroxyl and carbonyl relative intensity. Due to the formation of extra acetyl bridges between CA and PVA, the intensity of –OH will decrease, and the intensity of C═O carbonyl will increase. [37]. The OH/COOH ratio for the uncrosslinked polymer was 1.07 for HF0, while HF80-1 and HF130 were 0.89 and 0.77, respectively. The results indicated that the number of

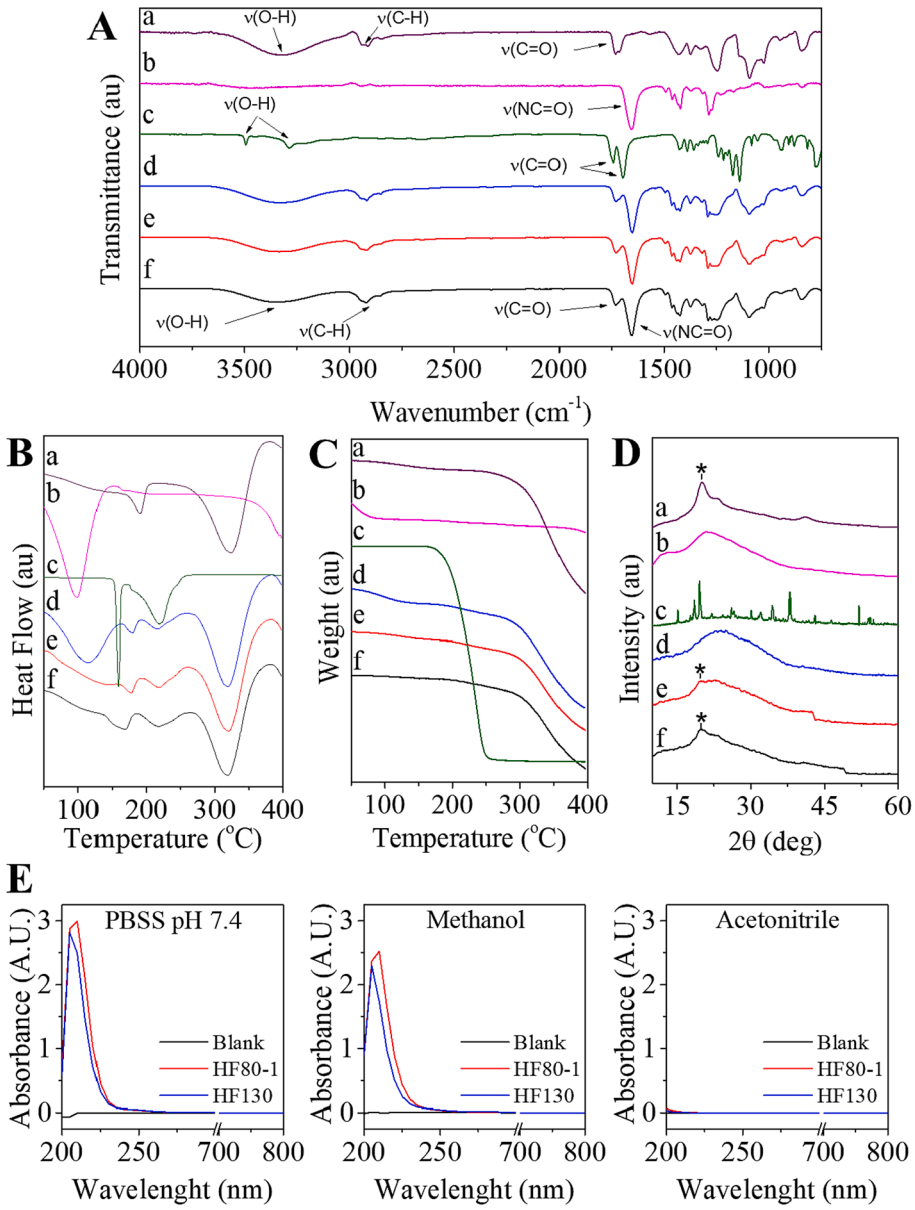

Fig. 4. Images of (A) ATR-FTIR spectra, (B) DSC thermogram, (C) TGA thermogram, (D) X-ray diffractogram and (E) UV–Vis spectra of the extractables. Annotation for figure (A) to (D) are: (a) Poly(vinyl alcohol) (PVA) 85–124 k; (b) Poly(vinylpyrrolidone) (PVP) K-29/32; (c) Citric Acid, Anhydrous; (d) HF0; (e) HF80-1; and (f) HF130.

hydroxyl groups in the hydrogel decreased because some ester bonds formed with the carboxyl group from the acid; hence, the crosslinking process was confirmed [33].

The thermograms of the hydrogel and its composition are given in Fig. 4B and 4C, and the thermal events are summarised in Table S5. The characteristic sharp endothermic peak of citric acid (~156 °C) that correlates to its melting event was not observed in the hydrogel, proving that CA was dispersed on a molecular level and did not recrystalize on the xerogel. However, its decomposition peak (~217 °C, confirmed by 100 % weight loss in the TGA thermogram) can still be seen in the hydrogel thermogram, which could indicate residual unreacted acid molecules [31]. A broad endothermic peak could be observed at ~ 98 °C for pure PVP and ~ 116 °C for HF0, mainly attributed to residual solvent and low molecular weight oligomer evaporation from PVP. This feature was not observed in HF80-1 and H130, indicating the complete removal of more volatile components during the crosslinking process. A different observed thermal event was the endothermic melting peak (without weight loss as confirmed by TGA) of pure PVA (~191 °C) [41,42]. This peak was not observed in the hydrogel samples, but instead, melting peaks at ~ 179 °C, ~177 °C and ~ 168 °C for HF0, HF80-1 and HF130 were observed (confirmed by the lack of weight loss on the TGA thermogram). This finding contradicts those reported in [37]. The crosslinking process is expected to increase the average molecular weight of the polymer, and it might raise the melting point of the crosslinked PVA polymer [37]. However, because the hydrogels that we studied are a composite, the interaction between the two macromolecules and citric acid might be the cause of the lower melting point of the crosslinked materials. As a glass transition temperature before the first melting events was detected, the two polymers can be regarded as a miscible mixture [43] with no indication of separation of the individual constituent.

The diffractograms comparing the solid-state characteristics of HF0, HF80-1 and HF130 are given in Fig. 4D. The results showed that the untreated hydrogel was primarily composed of an amorphous structure. The dried gel showed a hint of a crystalline phase demonstrated by a small peak at approximately 2θ of 19° that corresponded to the PVA

orthorhombic lattice that grows along with the [1 1 0] plane (annoted by * marks in the graph) [42]. Upon heating, the residual water inside the gel network will evaporate, further constricting the gel structure. In this case, the PVA chain comes into close contact and triggers crystallite and hydrogel bond formation [44]. We suggest that the crystalline region might form an intertwined structure, further embedding the PVP polymer strand into the hydrogel structure and preventing it from leaching out. No major diffraction peaks of CA [45] were observed in the hydrogels. Although the position of the most intense CA diffraction peak along the [1 0 2] plane is very close to the [1 1 0] peak of PVA, we believe the peak shown in the product hydrogel was attributed to the PVA crystalline peak. These results indicate that no unreacted CA crystallisation occurred inside the hydrogels, both before and after crosslinking.

The gel fraction calculated during the swelling study indicated that some constituent components were soluble in the swelling media. These compounds can be considered extractable. This study used three different solvents to study the extractable hydrogel components and then analysed them qualitatively using a spectrophotometer. The results of the spectral scan of the extraction solution are given in Fig. 4D. The graphs show a strong peak in the UV region with PBSS pH 7.4 and methanol as the solvent. The peaks were located in the same position for both hydrogels. The maximum absorbances were at ~ 205 nm for HF80-1 and ~ 210 nm for HF130. In contrast, the acetonitrile extract yielded no observable peaks in the UV and visible regions. It was clear that the extractables were polar molecules. This is not surprising, as the constituents of the composite are water-soluble compounds. Any impurities, such as residual solvents or oligomers, would be polar molecules. Possible impurities from the raw materials included polyvinyl acetate, acetic acid, and methyl acetate from PVA, as well as peroxides from PVP [46].

3.3. In vitro permeation, partitioning, and drug extraction study

Solute permeation across hydrogels was studied for 24 h, and the results are shown in Fig. 6A. For HF80-1, the cumulative permeation of the analytes was 79.60 ± 4.78 %, 64.21 ± 3.21 % and 71.32 ± 3.95 % for THEO, CYAN and FLUO, respectively. The cumulative permeation for THEO, CYAN and FLUO was 76.60 ± 0.71 %, 30.82 ± 1.46 % and 52.79 ± 54 %, respectively, for HF130. After 24 h, analyte permeation through HF130 was significantly lower ($p < 0.0001$), except for THEO ($p = 0.3645$), when compared with the HF80-1 permeation results. These findings demonstrate the effect of the crosslinking temperature on the permeation of the analyte. At higher temperatures, greater crosslinking degrees were achieved, which negatively impaired the hydrogel's permeability. The gel network will become denser at a higher crosslinking degree, and the mesh size will decrease, thus delaying analyte movement [47].

Another factor that needs to be considered is the difference in analyte chemical properties. The cumulative permeation of analytes through the same type of hydrogels was significantly different ($p < 0.0001$), except for THEO vs FLUO through HF80-1 ($p = 0.0004$) and CYAN vs FLUO through the HF80-1 hydrogel ($p = 0.0020$). THEO, CYAN and FLUO vary greatly in molecular size, solubility, hydrodynamic radius and physiological charge (Table S2). Interestingly, HF80-1 showed minor permeation variation between the analytes when compared to HF130, where the difference in cumulative permeation between each molecule is greater. The THEO molecular weight and hydrodynamic radius are the smallest among those of the other analytes (Table S2). After THEO, FLUO is the next and is then followed by CYAN in the order of molecular weight and hydrodynamic radius. It is not surprising that the order is also reflected in the permeation study, where THEO showed the highest permeation, followed by FLUO and then CYAN. This trend follows the Stokes-Einstein equation, where it was predicted that the permeation of the molecule would decrease as the molecular radius became larger [2].

Experimental calculations of the permeability (P), partition coefficient (K_d) and diffusion coefficient (D) are given in Table 2. Judging from the P values from both hydrogels, it is clear that the permeability follows the rule of the Stokes-Einstein equation, as the value is greater for smaller molecules and tends to be lower as the hydrodynamic radius increases [2]. The permeability measures the rate (distance over time) at which a drug molecule can travel across a membrane, in this case, the hydrogel membrane. Smaller molecules can travel freely without bumping into the polymeric network obstacles, thus having a high permeability constant.

Partitioning or the distribution coefficient heavily depends on the chemistry of the hydrogel and the chemistry of the molecule involved. The PVA molecule is considered neutral, but at a certain pH, the residual acetate group could give it a net negative charge. In contrast, the PVP molecule has a pH-dependent charge behavior where a positive surface charge will occur at a lower pH [48]. Based on the measurement of surface pH discussed before, it can be speculated that the internal environment of the hydrogel is acidic, thus allowing the functional groups of the PVP polymer to be positively charged and providing ionic interaction sites for permeating molecules.

The results of analyte uptake and extraction yield are given in Fig. 5B and 6C, and the calculation of the coefficient of determination (R^2) is summarised in Table 3. Linear responses of analyte extraction were noticed in this study in all model molecules with $R^2 > 0.98$, which means that the results are concentration dependent. The higher the concentration of analyte, the more molecules the hydrogel could take up. A similar response was also observed in the uptake study but with poorer linearity.

The graphs show that HF80-1 was able to absorb more molecules than HF130, which is consistent with the K_d values measured for both hydrogel formulations. This result strengthens the evidence that the properties of the target molecule play a significant role in the performance of these hydrogels. HF80-1 could be considered to perform better because it has a steeper slope in the regression curves (compared to HF130 curves), indicating that it has better sensitivity in both the amount of drug sampled and the recovery efficiency.

3.4. Microneedle array patch fabrication and characterisation

MAPs were examined using a stereomicroscope and a scanning electron microscope. The results are given in Fig. 6A. Upon microscopic examination, it was clearly seen that the MAPs were successfully demoulded by the intact needle and patch. All needles were pyramidal and did not undergo shape deformation after heating. The results of the needle height calculations are given in Figure S. This study demonstrated that the needle would shrink after thermal treatment, resulting in a difference in needle height. HF80-1 MAPs were significantly longer than HF130 MAPs ($p < 0.0001$).

HF80-1 and HF130 MAPs demonstrated comparable mechanical properties (illustration is given in Fig. 9B). At 10 N/array (equivalent to 0.05 N per needle), the needles were deformed (not broken) with an average height reduction of 4.2 ± 2.2 % and 3.6 ± 2.3 % for HF80-1 and HF130, respectively, where the uncrosslinked array needles were reduced by a magnitude of 6.4 ± 2.4 % from their original height. The

Table 2
Permeability and partitioning parameters from hydrogel formulation.

Drug	HF80-1			HF130		
	P*	K_d	D**	P*	K_d	D**
THEO	7.43 ± 1.10	1.30 ± 0.01	16.17	5.45 ± 0.36	2.23 ± 0.34	4.77
FLUO	4.71 ± 1.24	5.68 ± 0.45	2.32	1.71 ± 0.07	3.79 ± 0.54	0.88
CYAN	2.54 ± 0.29	0.98 ± 0.12	7.31	0.91 ± 0.05	0.52 ± 0.03	3.44

* = x 10^{-5} cm/s, ** = x 10^{-6} cm^2/s.

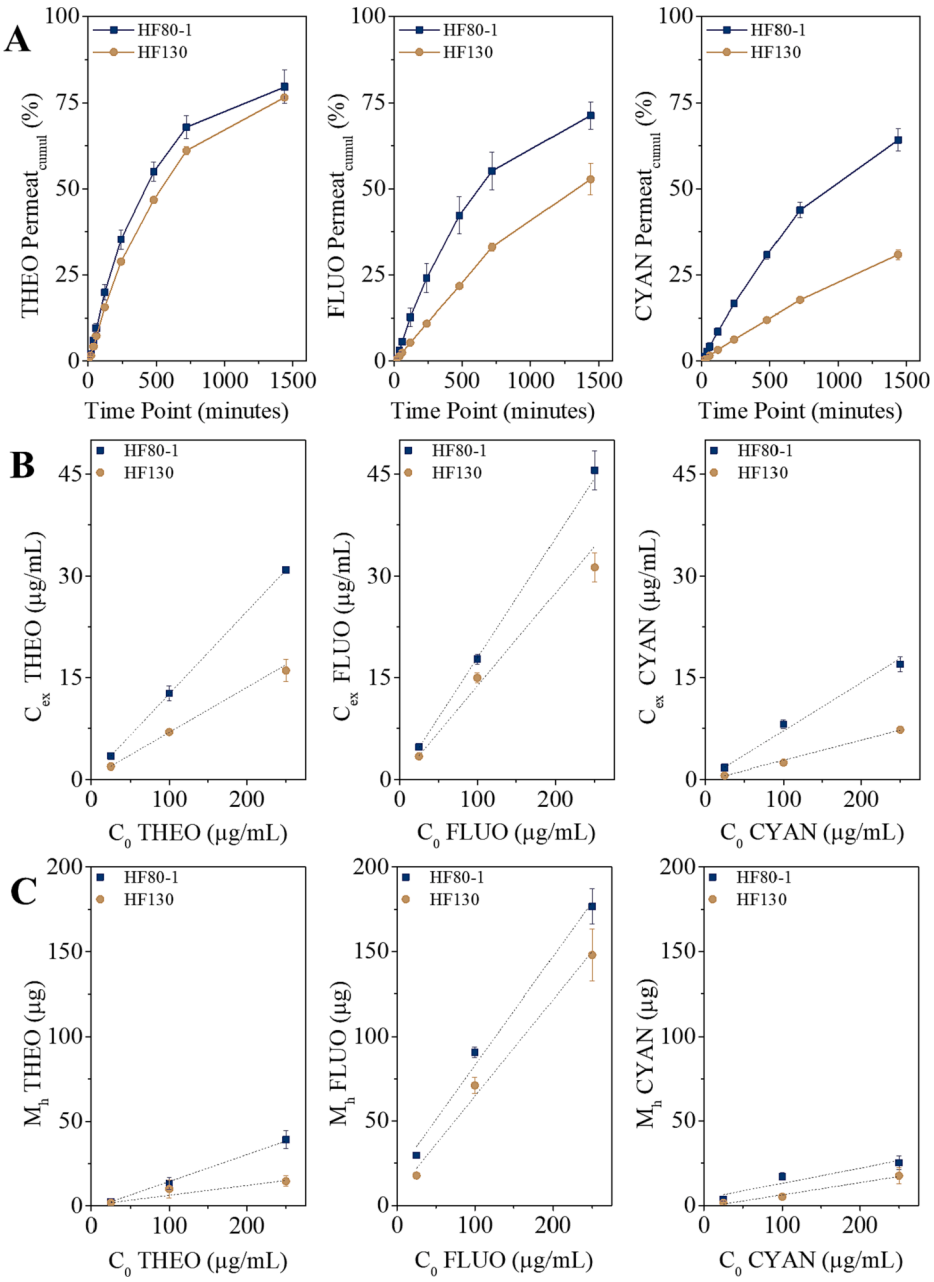

Fig. 5. Plot of (A) permeation curve of molecules through HF80-1 and HF130 tested on horizontal diffusion cells, (B) analyte extraction recovery by a simple extraction process; and (C) calculated analyte uptake by hydrogels (means ± SDs, n = 3).

height reduction of HF80-1 and HF130 was not statistically significant ($p = 0.6747$). At the 32/N array (equivalent to 0.16 N/array), all patches, including the uncrosslinked formulation, showed the same compressive strength, where the needles' height reduction was ~ 10 % after the test. These results indicate that the end part of the needle tips was stronger after crosslinking, but the gross height reduction was similar at 32 N/array.

The penetration of microneedles through a stack of eight layers of Parafilm M® was used to gauge the insertion of MAPs through skin. Parafilm M® was proposed as a model membrane to be used in a routine test for MAPS insertion [27]. The results of this test are shown in Fig. 6C, and the OCT image representation is given in Fig. 6D. At a force of 32 N/patch, the effect of formulation on the depth of insertion was not statistically significant ($p = 0.2379$, evaluated on the 3rd Parafilm M® layer). OCT imaging of ex vivo skin insertion revealed that both HF80-1 and HF130 MAPS could pierce the epidermal layer and be inserted well into the skin. At a closer look, there were air spaces between HF130 MAPs with the skin, but the same thing was not observed in the HF80-1 formulation.

3.5. *Ex vivo* drug monitoring test

Ex vivo drug monitoring tests were carried out using a modified Saarbrücken model, and the results are given in Fig. 7. In this model, excised neonatal porcine skin pieces were equilibrated with a drug solution for 3.5 h. After preincubation, the amount of free drug in the ISF was quantified. The ISF was separated from the tissue using centrifugation, and the results are shown in Fig. 7A. It was observed that the concentration of free THEO and CYAN found in the ISF (C-ISF$_{free}$) was proportional to the concentration of drugs in the soaking solution (C-solution$_0$). Interestingly, only a small amount of free FLUO can be detected in the ISF, possibly due to its ability to redistribute itself to the

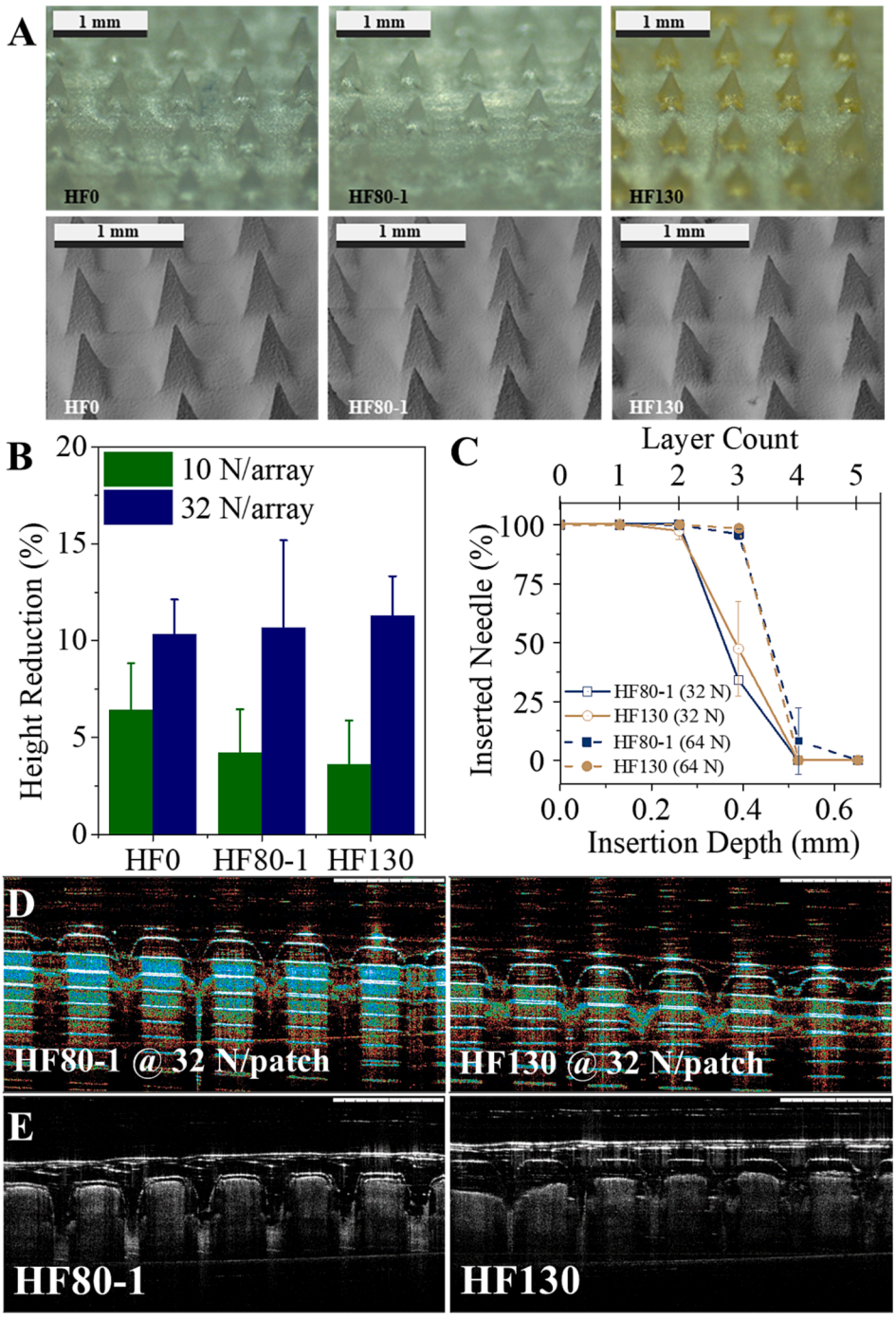

Fig. 6. (A) Representative image of each MAP taken with light microscopy (35x magnification) and SEM (100x magnification); (B) Needle height reduction test results represented as the percentage of the reduction of needle tips (means ± SDs, n = 5). (C) Parafilm M® insertion study results as a graph of the depth of penetration. (D) OCT image representation of the Parafilm M® insertion study. (E) OCT images of skin *ex vivo* insertion studies using manual thumb force.

intracellular portion of the skin [49] after several hours of soaking.

In the *ex vivo* drug monitoring evaluation, the MAPs were applied for 1 h. After 1 h, the patch was removed and extracted using a simple and nondestructive method by soaking it in an extraction solution followed by manual shaking. This separation technique has been used to monitor lithium concentration using hydrogel-forming microneedles [10]. Although the trend can be seen in the graph (Fig. 7), these results did not show any significant difference when evaluated using an unpaired *t* test (p for THEO = 0.1707, FLUO = 0.1654, and CYAN = 0.1136) due to variation possibly coming from the experimental setup.

3.6. *Ex vivo* delivery study

This study demonstrates the ability of polymeric HF-MAPs tandem with PEG reservoirs to deliver drugs. The melt-type reservoir was a PEG-based system specifically formulated to melt around the skin's surface temperature. The melt-type reservoir is designed to melt within minutes, essentially providing a liquid drug layer above the hydrogel, allowing drug diffusion to occur immediately after melting. After a preliminary screening using different molecular weight PEG, a combination of PEG 400 and PEG 1000 at 1:9 was satisfactory and, therefore, used in this study.

Table 3
Summary of the linearity (stated as R^2) of the extraction and analyte uptake experiments calculated based on the graph represented in Fig. 5B and 5C.

Analyte	Hydrogel	Coefficient of determination	
		Extraction	Uptake
THEO	HF80-1	0.9976	0.9616
	HF130	0.9818	0.8467
CYAN	HF80-1	0.9818	0.9064
	HF130	0.9919	0.6831
FLUO	HF80-1	0.9929	0.9831
	HF130	0.9829	0.9853

Fig. 8A provides the visual representation and the results from the melting time evaluation of each drug reservoir. The drug to polymer ratio was 1:9, omitting the solubility of each drug in the carrier. Upon close observation, it was clear that the drug particles were partially soluble, and the nonsalable particles were dispersed on the carrier. Each reservoir was melted within 2 min when placed on top of the preswollen warmed hydrogel. The effect of different loaded drugs on the melting time was not statistically significant ($p > 0.1$), except for CYAN, where the melting time was slightly longer than that of the blank PEG reservoir ($p = 0.0213$).

The DSC thermogram (Fig. 8B) shows that the reservoir's melting point was ≤ 30 °C. In the pure form, PEG 1000 melts at approximately 37.1 °C [50], but adding PEG 400 lowers its melting point. The drug addition decreased the melting point to ~ 1.6 °C lower than that of the PEG blank base. This PEG mixture also has a broad melting transition because lighter PEG possesses an earlier melting onset and broader phase transition interval [50]. Another early endothermic peak was found at approximately 24–25.6 °C in the drug-containing reservoir but not in the blank PEG samples. This is possibly due to phase separation caused by the imperfect solubility of the drug inside the matrix. The ATR-FTIR study revealed the interaction between PEG and drugs (Fig. 8C). As PEG was the principal constituent, only the PEG-related peak can be seen clearly in the functional group area. The vibrational modes at ~ 2870 cm^{-1} and ~ 3440 cm^{-1} correspond to C—H and O—H vibrations on the PEG polymeric chain [51].

The results of the *ex vivo* drug delivery study using the Franz Cell apparatus are given in Fig. 8D, and the results of the skin and hydrogel drug deposition studies are given in Fig. 8E. At the 30-minute time point, the number of drugs permeating through the receptor compartment reached 10.6 ± 3.1 μg, 1.0 ± 0.3 and 8.3 ± 7.1 μg in 12 ml for THEO, FLUO and CYAN, respectively. This trend continued until 24 h, when the cumulative permeation reached 4043.3 ± 399.9 μg, 610.7 ± 120.2 μg, and 1755.3 ± 303.1 μg in 12 ml for THEO, FLUO and CYAN, respectively. Plugging the results over 24 h into four different kinetic models, namely, zero-order, first-order, Higuchi and Korsmeyer-Peppas equations, it is clear that the delivery kinetics fit into the Korsmeyer-Peppas model with R^2 value > 0.99 and the zero-order kinetics came as the second closest with R^2 value > 0.96 (Table 4). A further assessment to take lag time into account was made. The results were the same: all three drugs' diffusion kinetics followed the Korsmeyer-Peppas model with improved linearity with $R^2 > 0.998$ (Table 4 and Table 5), showing a possible initial lag time involved during the in vitro evaluation. This lag time can be attributed to several factors, such as the reservoir's initial melting/dissolution time and the time the hydrogel takes to hydrate and swell. An illustration of the possible contribution of various factors involved in the delivery system, including the lag time, is given in Fig. 9.

Evaluating the drug deposition, it was clear that only a minimal amount of drug resided inside the skin. The difference in the amount of drug extracted from the skin using PBS solution pH 7.4 was insignificant compared to each other ($p > 0.1$). Due to the hydrophilic nature of the drug, the molecule will permeate the skin mainly through the intercellular route where water is abundant, with a small quantity that might permeate through the transcellular route, depending on their LogP value.

The amount of drug found in the hydrogels was several-fold higher than that in the skin, highlighting the high affinity of hydrophilic drugs to interact with polymeric PVA/PVP/CA HF-MAPs. As the drugs are soluble in water, which is mediated by hydrogen bond interactions, they can also form a strong hydrogen bond or even ionic interaction with the hydrogel. It is important to note that the magnitude of extracted drugs reported here is an underestimation. Due to the partitioning effect, it is impossible to extract 100 % of the entrapped drug in the hydrogel matrix with a water-based solvent even though we physically disrupted the macroscopic structure of the material. Such an effect can only be achieved using solvents where the drug has a higher affinity to dissolve [10], but it is beyond the scope of this work. Nevertheless, the results can capture the overall extreme ratio between the extent of drug molecules residing in the hydrogel and the skin.

FLUO showed the lowest initial and cumulative delivery after 24 h, although its solubility is > 45-fold higher than those of the other two drugs and has a smaller hydrodynamic radius than CYAN. From the permeation study, it is clear that HF80-1 is less selective to molecule size than HF130, possibly due to its larger mesh size and less intricate network structure. Hydrogels with a lower crosslinking ratio will result in a more permeable attribute. Therefore, different factors should play roles in determining the total drug delivered overall.

Based on the assumption above, we look into several experimental data and plot the values against the cumulative permeation to see whether they are correlated. From the assessment (as illustrated in Fig. 9), it is clear that the degree of diffusion coefficient (D) seems to

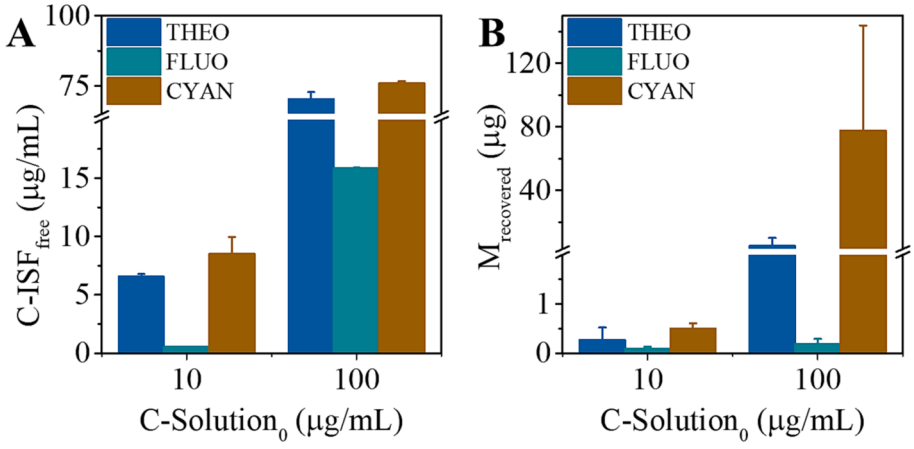

Fig. 7. Results of (A) drug concentration quantification in the neonatal porcine skin extracellular fluid after 3.5 h of preincubation at 37 °C and (B) drug concentrations in the extraction fluid of HF-MAPs after 1-hour application in the drug-impregnated neonatal porcine skin (means ± SDs, n = 3).

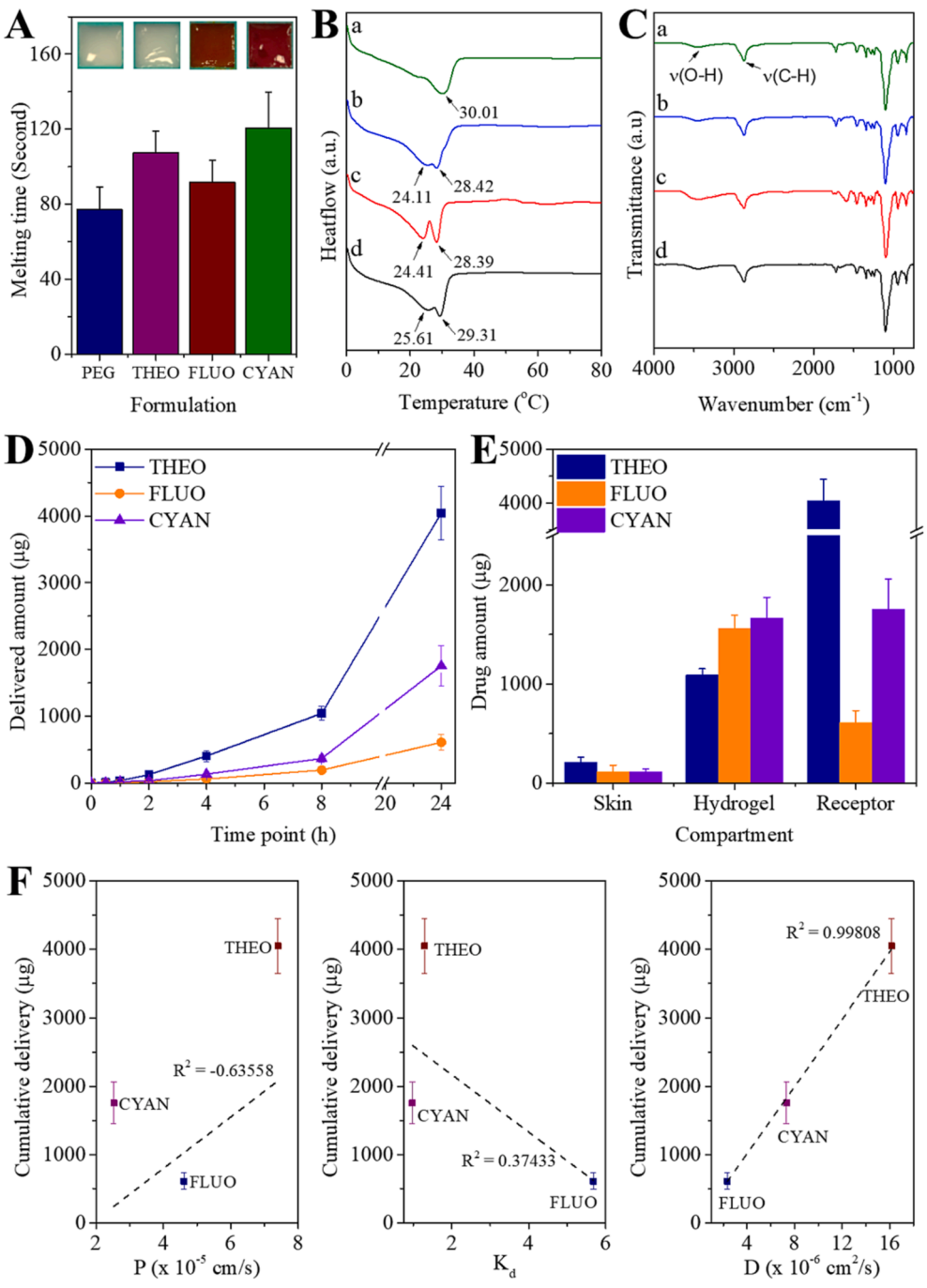

Fig. 8. Image of (A) melting time study, (B) DSC thermogram, and (C) ATR-FTIR spectrum of the reservoirs. Annotations for Figure (B) and (C) are (a) blank PEG reservoir consisting of PEG 400 and PEG 1000 1:9; (b) THEO-PEG reservoir; (c) FLUO-PEG reservoir, and (f) CYAN-PEG reservoir. (D) Delivery profile of three different model drugs across neonatal full-thickness skin. (E) Comparison of drugs deposited in the skin, remaining in the hydrogel, and delivered in the receptor compartment after 24 h. (F) Relationship between the cumulative delivery amount of model drugs vs their permeability, partitioning and diffusion coefficient with respect to the HF80-1 hydrogel formulation (means ± SDs, n = 3). (For interpretation of the references to colour in this figure legend, the reader is referred to the web version of this article.)

correlate linearly with the average cumulative permeation after 24 h. The D value seems to be a good predictive value to determine how efficiently a hydrophilic drug can be delivered through this PVA/PVP/CA hydrogel formulation, as it considers both the rate at which the drug molecules travel across the hydrogel and their tendency to interact with the polymeric material. Strongly interacting drugs modelled by FLUO might not be suitable for PVA/PVP/CA-based HF-MAPs, as many drugs will be trapped inside the array rather than delivered to the skin. THEO represents the ideal drug because it possesses both high permeability and low partitioning, making it efficiently delivered using these polymeric HF-MAPs. Overall, the investigation carried out in this study showed the effectiveness of HF-MAPs to deliver hydrophilic compounds transdermally after the modification of crosslinking conditions. Essentially, the interaction between hydrophilic drugs and hydrogel, observed using several techniques explained previously, could potentially be used to predict the permeation patterns of the drug integrated with HF-MAPs. Therefore, this could be applied in the development of the transdermal delivery of hydrophilic compounds.

4. Conclusion

The work presented here describes, for the first time, the preparation and characterisation of PVA/PVP/CA HF-MAPs crosslinked at 80 °C. The hydrogel shows good permeability, and the HF-MAP formulation possesses sufficient mechanical strength to aid skin insertion. This work reports *ex vivo* drug monitoring using a modified Saarbrücken model and an *ex vivo* drug delivery study using a melt-type reservoir. The *ex vivo* results demonstrate the ability to perform drug monitoring using this

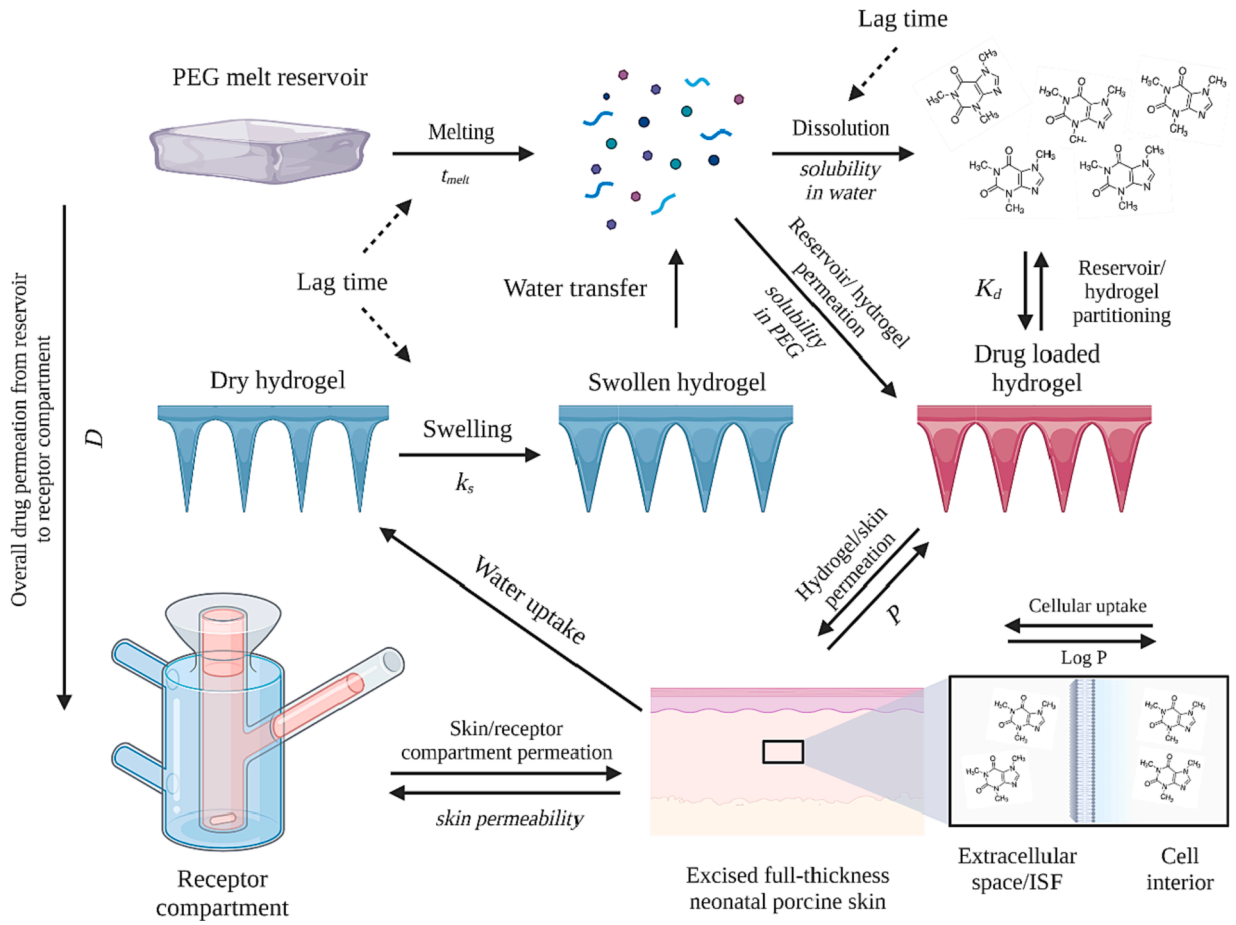

Fig. 9. Illustration of the proposed *ex vivo* drug delivery mechanism using PVA/PVP/CA HF-MAPs in tandem with melt-type reservoirs. This illustration includes the proposed possible factor contributing to the whole delivery kinetics at each stage and the proposed contributing factor to the lag time observed in the experiment. The text above the arrow indicates the process, and the italic text below the arrow represents the contributing factor taking place in the process.

Table 4
Evaluation of R^2 values from drug delivery model fitting using DDSolver.

Drug Model	Kinetic Model					
	0th order	1st order	Higuchi	Korsmeyer-Peppas	0th order with T_{lag}	Korsmeyer-Peppas with T_{lag}
THEO	0.9818	−0.3485	0.7322	0.9986	0.9941	0.9996
FLUO	0.9868	0.0409	0.7556	0.9948	0.9956	0.9984
CYAN	0.9672	−0.2036	0.6979	0.9998	0.9867	0.9999

Table 5
Korsmeyer-Peppas parameter estimation from the drug delivery profile.

Drug Model	T_{lag} (min)	kKP (min^{-1})	n	Remark
THEO	43.087	1.522	1.173	Super Case-II Transport
FLUO	85.495	0.799	0.972	Anomalous
CYAN	19.123	0.104	1.385	Super Case-II Transport

type of HF-MAP with a simple extraction method. The delivery study shows the potential use of a melt-type reservoir in conjunction with this polymeric HF-MAP formulation. Based on the results, we suggest that hydrophilic drug interactions play a great role in the application of PVA/PVP/CA-based HF-MAPs.

CRediT authorship contribution statement

Achmad Himawan: Conceptualization, Data curation, Investigation, Methodology, Project administration, Validation, Visualization, Writing – original draft. **Qonita Kurnia Anjani:** Investigation, Methodology. **Usanee Detamornrat:** Conceptualization, Investigation, Methodology, Writing – review & editing. **Lalitkumar K. Vora:** Conceptualization, Writing – review & editing. **Andi Dian Permana:** Conceptualization, Writing – review & editing. **Rand Ghanma:** Investigation, Methodology. **Yara Naser:** Conceptualization, Investigation, Methodology. **Dina Rahmawanty:** Investigation. **Christopher J. Scott:** Conceptualization, Supervision, Writing – review & editing. **Ryan F. Donnelly:** Conceptualization, Funding acquisition, Methodology, Project administration, Resources, Supervision, Writing – review & editing.

Declaration of Competing Interest

The authors declare the following financial interests/personal relationships which may be considered as potential competing interests: Ryan Donnelly is an inventor of patents that have been licenced to companies developing microneedle-based products and is a paid advisor

to companies developing microneedle-based products. The resulting potential conflict of interest has been disclosed and is managed by Queen's University Belfast. The companies had no role in the design of the present studies, in the collection, analyses or interpretation of the data, in the writing of the manuscript or in the decision to publish the work. Other all authors declare that they have no known competing financial interests or personal relationships that could have appeared to influence the work reported in this paper..

Data availability

Data will be made available on request.

Acknowledgement

The authors thankfully acknowledge the financial support of the CITI-GENS programme at Queen's University Belfast, co-funded with the EU Horizon 2020 scheme under the Marie Sklodowska-Curie Action grant agreement Number 945231 – CITI-GENS. Original illustrations are made with Biorender.

Data availability

Data available upon request

Appendix A. Supplementary material

Supplementary data to this article can be found online at https://doi.org/10.1016/j.eurpolymj.2023.111836.

References

[1] T.R.R. Singh, P.A. McCarron, A.D. Woolfson, R.F. Donnelly, Investigation of swelling and network parameters of poly(ethylene glycol)-crosslinked poly(methyl vinyl ether-co-maleic acid) hydrogels, Eur. Polym. J. 45 (2009) 1239–1249, https://doi.org/10.1016/J.EURPOLYMJ.2008.12.019.

[2] T.R.R. Singh, A.D. Woolfson, R.F. Donnelly, Investigation of solute permeation across hydrogels composed of poly(methyl vinyl ether-co-maleic acid) and poly (ethylene glycol), J. Pharm. Pharmacol. 62 (2010) 829–837, https://doi.org/10.1211/jpp.62.07.0003.

[3] A. Léonard, S. Blacher, M. Crine, W. Jomaa, Evolution of mechanical properties and final textural properties of resorcinol–formaldehyde xerogels during ambient air drying, J. Non Cryst. Solids 354 (2008) 831–838, https://doi.org/10.1016/J.JNONCRYSOL.2007.08.024.

[4] R.F. Donnelly, T.R.R. Singh, M.J. Garland, K. Migalska, R. Majithiya, C. M. McCrudden, et al., Hydrogel-Forming Microneedle Arrays for Enhanced Transdermal Drug Delivery, Adv. Funct. Mater. 22 (2012) 4879–4890, https://doi.org/10.1002/ADFM.201200864.

[5] R.F. Donnelly, M.T.C. McCrudden, A.Z. Alkilani, E. Larrañeta, E. McAlister, A. J. Courtenay, et al., Hydrogel-Forming Microneedles Prepared from "Super Swelling" Polymers Combined with Lyophilised Wafers for Transdermal Drug Delivery, PLoS One 9 (2014), e111547, https://doi.org/10.1371/journal.pone.0111547.

[6] J.G. Turner, L.R. White, P. Estrela, H.S. Leese, J.G. Turner, L.R. White, et al., Hydrogel-Forming Microneedles: Current Advancements and Future Trends, Macromol. Biosci. 21 (2021) 2000307, https://doi.org/10.1002/MABI.202000307.

[7] K. Cheung, D. Das, Microneedles for drug delivery: trends and progress, Drug Delivery 23 (2016) 2338–2354, https://doi.org/10.3109/10717544.2014.986309.

[8] Y.A. Gomaa, D.I.J. Morrow, M.J. Garland, R.F. Donnelly, L.K. El-Khordagui, V. M. Meidan, Effects of microneedle length, density, insertion time and multiple applications on human skin barrier function: Assessments by transepidermal water loss, Toxicol. Vitr. 24 (2010) 1971–1978, https://doi.org/10.1016/J.TIV.2010.08.012.

[9] R. Al-Kasasbeh, A.J. Brady, A.J. Courtenay, E. Larrañeta, M.T.C. McCrudden, D. O'Kane, et al., Evaluation of the clinical impact of repeat application of hydrogel-forming microneedle array patches, Drug Deliv. Transl. Res. 10 (2020) 690–705, https://doi.org/10.1007/S13346-020-00727-2.

[10] E. Eltayib, A.J. Brady, E. Caffarel-Salvador, P. Gonzalez-Vazquez, A. Zaid Alkilani, H.O. McCarthy, et al., Hydrogel-forming microneedle arrays: Potential for use in minimally-invasive lithium monitoring, Eur. J. Pharm. Biopharm. 102 (2016) 123–131, https://doi.org/10.1016/j.rser.2016.01.089.

[11] E. Caffarel-Salvador, A.J. Brady, E. Eltayib, T. Meng, A. Alonso-Vicente, P. Gonzalez-Vazquez, et al., Hydrogel-forming microneedle arrays allow detection of drugs and glucose in vivo: Potential for use in diagnosis and therapeutic drug monitoring, PLoS One 10 (2015) 1–21, https://doi.org/10.1371/journal.pone.0145644.

[12] R.F. Donnelly, T.R.R. Singh, A.Z. Alkilani, M.T.C. McCrudden, S. O'Neill, C. O'Mahony, et al., Hydrogel-forming microneedle arrays exhibit antimicrobial properties: Potential for enhanced patient safety, Int. J. Pharm. 451 (2013) 76–91, https://doi.org/10.1016/J.IJPHARM.2013.04.045.

[13] E. McAlister, B. Dutton, L.K. Vora, L. Zhao, A. Ripolin, D.S.Z.B.P.H. Zahari, et al., Directly Compressed Tablets: A Novel Drug-Containing Reservoir Combined with Hydrogel-Forming Microneedle Arrays for Transdermal Drug Delivery, Adv. Healthc. Mater. 10 (2021) 2001256, https://doi.org/10.1002/ADHM.202001256.

[14] K. Peng, L.K. Vora, J. Domínguez-Robles, Y.A. Naser, M. Li, E. Larrañeta, et al., Hydrogel-forming microneedles for rapid and efficient skin deposition of controlled release tip-implants, Mater. Sci. Eng. C 127 (2021), 112226, https://doi.org/10.1016/J.MSEC.2021.112226.

[15] S. Huang, H. Liu, S. Huang, T. Fu, W. Xue, R. Guo, Dextran methacrylate hydrogel microneedles loaded with doxorubicin and trametinib for continuous transdermal administration of melanoma, Carbohydr. Polym. 246 (2020), 116650, https://doi.org/10.1016/J.CARBPOL.2020.116650.

[16] Y. Tang, S. Li, L. Hu, X. Sun, B. Zhang, W. Ji, et al., Hybrid Poly(AMPS-CS)-Au Microneedle Arrays to Enrich Metabolites from Skin for Early Disease Diagnosis, Adv. Healthc. Mater. 10 (2021) 2100764, https://doi.org/10.1002/adhm.202100764.

[17] L.K. Vora, K. Moffatt, I.A. Tekko, A.J. Paredes, F. Volpe-Zanutto, D. Mishra, et al., Microneedle array systems for long-acting drug delivery, Eur. J. Pharm. Biopharm. 159 (2021) 44–76, https://doi.org/10.1016/J.EJPB.2020.12.006.

[18] I.A. Tekko, G. Chen, J. Domínguez-Robles, R.R.S. Thakur, I.M.N. Hamdan, L. Vora, et al., Development and characterisation of novel poly (vinyl alcohol)/poly (vinyl pyrrolidone)-based hydrogel-forming microneedle arrays for enhanced and sustained transdermal delivery of methotrexate, Int. J. Pharm. 586 (2020), 119580, https://doi.org/10.1016/J.IJPHARM.2020.119580.

[19] Q.K. Anjani, A.D. Permana, Á. Cárcamo-Martínez, J. Domínguez-Robles, I. A. Tekko, E. Larrañeta, et al., Versatility of hydrogel-forming microneedles in in vitro transdermal delivery of tuberculosis drugs, Eur. J. Pharm. Biopharm. 158 (2021) 294–312, https://doi.org/10.1016/J.EJPB.2020.12.003.

[20] N. Xu, M. Zhang, W. Xu, G. Ling, J. Yu, P. Zhang, Swellable PVA/PVP hydrogel microneedle patches for the extraction of interstitial skin fluid toward minimally invasive monitoring of blood glucose level, Analyst 147 (2022) 1478–1491, https://doi.org/10.1039/D1AN02288A.

[21] I. Barandiaran, J. Gutierrez, A. Tercjak, G. Kortaberria, Effect of γ-Fe2O3 nanoparticles on the cross-linking and final properties of PVA/Citric Acid-based nanocomposites, J. Phys. Chem. C 124 (2020) 5444–5451, https://doi.org/10.1021/ACS.JPCC.9B11219.

[22] Z. Czibulya, A. Csík, F. Tóth, P. Pál, I. Csarnovics, R. Zelkó, et al., The Effect of the PVA/Chitosan/Citric Acid Ratio on the Hydrophilicity of Electrospun Nanofiber Meshes, Polym 13 (2021) 3557, https://doi.org/10.3390/POLYM13203557.

[23] M.T. Khorasani, A. Joorabloo, A. Moghaddam, H. Shamsi, Z. MansooriMoghadam, Incorporation of ZnO nanoparticles into heparinised polyvinyl alcohol/chitosan hydrogels for wound dressing application, Int. J. Biol. Macromol. 114 (2018) 1203–1215, https://doi.org/10.1016/J.IJBIOMAC.2018.04.010.

[24] I. Nozawa, Y. Suzuki, S. Sato, K. Sugibayashi, Y. Morimoto, Preparation of thermo-responsive polymer membranes. I, J. Biomed. Mater. Res. 25 (1991) 243–254, https://doi.org/10.1002/JBM.820250210.

[25] J.M. Yang, W.Y. Su, T.L. Leu, M.C. Yang, Evaluation of chitosan/PVA blended hydrogel membranes, J. Memb. Sci. 236 (2004) 39–51, https://doi.org/10.1016/J.MEMSCI.2004.02.005.

[26] I.K. Ramöller, E. McAlister, A. Bogan, A.S. Cordeiro, R.F. Donnelly, Novel design approaches in the fabrication of polymeric microarray patches via micromoulding, Micromachines 11 (2020) 554, https://doi.org/10.3390/MI11060554.

[27] E. Larrañeta, J. Moore, E.M. Vicente-Pérez, P. González-Vázquez, R. Lutton, A. D. Woolfson, et al., A proposed model membrane and test method for microneedle insertion studies, Int. J. Pharm. 472 (2014) 65–73, https://doi.org/10.1016/J.IJPHARM.2014.05.042.

[28] H. Wagner, K.H. Kostka, C.M. Lehr, U.F. Schaefer, Interrelation of permeation and penetration parameters obtained from in vitro experiments with human skin and skin equivalents, J. Control. Release 75 (2001) 283–295, https://doi.org/10.1016/S0168-3659(01)00396-0.

[29] Y. Zhang, M. Huo, J. Zhou, A. Zou, W. Li, C. Yao, et al., DDSolver: An Add-In Program for Modeling and Comparison of Drug Dissolution Profiles, AAPS J. 12 (2010) 263, https://doi.org/10.1208/S12248-010-9185-1.

[30] A. Das, R. Uppaluri, C. Das, Feasibility of poly-vinyl alcohol/starch/glycerol/citric acid composite films for wound dressing applications, Int. J. Biol. Macromol. 131 (2019) 998–1007, https://doi.org/10.1016/J.IJBIOMAC.2019.03.160.

[31] M. Sabzi, M.J. Afshari, M. Babaahmadi, N. Shafagh, pH-dependent swelling and antibiotic release from citric acid crosslinked poly(vinyl alcohol) (PVA)/nano silver hydrogels, Colloids Surfaces B Biointerfaces 188 (2020), 110757, https://doi.org/10.1016/J.COLSURFB.2019.110757.

[32] S. Thongsuksaengcharoen, S. Samosorn, K. Songsrirote, A facile synthesis of self-catalytic hydrogel films and their application as a wound dressing material coupled with natural active compounds, ACS Omega 5 (2020) 25973, https://doi.org/10.1021/ACSOMEGA.0C03414.

[33] A.K. Sonker, K. Rathore, R.K. Nagarale, V. Verma, Crosslinking of Polyvinyl Alcohol (PVA) and Effect of Crosslinker Shape (Aliphatic and Aromatic) Thereof, J. Polym. Environ. 26 (2018) 1782–1794, https://doi.org/10.1007/S10924-017-1077-3.

[34] I. Van Nieuwenhove, A. Salamon, K. Peters, G.J. Graulus, J.C. Martins, D. Frankel, et al., Gelatin- and starch-based hydrogels. Part A: Hydrogel development,

characterization and coating, Carbohydr. Polym. 152 (2016) 129–139, https://doi.org/10.1016/J.CARBPOL.2016.06.098.
[35] J. Gohil, P. Ray, Studies on oxalic acid as a crosslinker of polyvinyl alcohol, Polymers and Polymer, Composite 17 (2009) 403–410, https://doi.org/10.1177/096739110901700702.
[36] E. Nicol, Photopolymerized Porous Hydrogels, Biomacromolecules 22 (2021) 1325–1345, https://doi.org/10.1021/acs.biomac.0c01671.
[37] D. Nataraj, R. Reddy, N. Reddy, Crosslinking electrospun poly (vinyl) alcohol fibers with citric acid to impart aqueous stability for medical applications, Eur. Polym. J. 124 (2020), 109484, https://doi.org/10.1016/J.EURPOLYMJ.2020.109484.
[38] A.M. Abdelghany, E.M. Abdelrazek, S.I. Badr, M.A. Morsi, Effect of gamma-irradiation on (PEO/PVP)/Au nanocomposite: Materials for electrochemical and optical applications, Mater. Des. 97 (2016) 532–543, https://doi.org/10.1016/J.MATDES.2016.02.082.
[39] H.M. Zidan, E.M. Abdelrazek, A.M. Abdelghany, A.E. Tarabiah, Characterization and some physical studies of PVA/PVP filled with MWCNTs, J. Mater. Res. Technol. 8 (2019) 904–913, https://doi.org/10.1016/J.JMRT.2018.04.023.
[40] S.A. Brandán, L.C. Bichara, H.E. Lans, E.G. Ferrer, M.B. Gramajo, Vibrational study and force field of the citric acid dimer based on the SQM methodology, Adv. Phys. Chem. 2011 (2011) 1–10, https://doi.org/10.1155/2011/347072.
[41] N.A. Betti, Thermogravimetric analysis on PVA/PVP blend under air atmosphere, Eng Tech J 34 (2016) 2433–2441.
[42] J. Zhu, Q. Li, Y. Che, X. Liu, C. Dong, X. Chen, et al., Effect of Na2CO3 on the microstructure and macroscopic properties and mechanism analysis of PVA/CMC composite film, Polymers (Basel) 12 (2020) 453, https://doi.org/10.3390/POLYM12020453.
[43] S. Sheik, G.K. Nagaraja, K. Prashantha, Effect of silk fiber on the structural, thermal, and mechanical properties of PVA/PVP composite films, Polym. Eng. Sci. 58 (2018) 1923–1930, https://doi.org/10.1002/PEN.24801.
[44] J.L. Holloway, A.M. Lowman, G.R. Palmese, The role of crystallization and phase separation in the formation of physically cross-linked PVA hydrogels, Soft Matter 9 (2012) 826–833, https://doi.org/10.1039/C2SM26763B.
[45] N. Kalaimani, K. Ramya, G. Vinitha, R. Aarthi, C.R. Raja, Structural, spectral, thermal and nonlinear optical analysis of anhydrous citric acid crystal, Optik 192 (2019) 162960, https://doi.org/10.1016/j.ijleo.2019.162960.
[46] Y. Wu, J. Levons, A.S. Narang, K. Raghavan, V.M. Rao, Reactive impurities in excipients: Profiling, identification and mitigation of drug–excipient incompatibility, AAPS PharmSciTech 12 (2011) 1248–1263, https://doi.org/10.1208/S12249-011-9677-Z.
[47] A. Cavallo, M. Madaghiele, U. Masullo, M.G. Lionetto, A. Sannino, Photo-crosslinked poly(ethylene glycol) diacrylate (PEGDA) hydrogels from low molecular weight prepolymer: Swelling and permeation studies, J. Appl. Polym. Sci. 134 (2017) 44380, https://doi.org/10.1002/APP.44380.
[48] N. Wang, Y. Feng, Y. Zheng, L. Zhang, M. Feng, X. Li, et al., New Hydrogen Bonding Enhanced Polyvinyl Alcohol Based Self-Charged Medical Mask with Superior Charge Retention and Moisture Resistance Performances, Adv. Funct. Mater. 31 (2021) 2009172, https://doi.org/10.1002/ADFM.202009172.
[49] L.D. Swindle, S.G. Thomas, M. Freeman, P.M. Delaney, View of Normal Human Skin In Vivo as Observed Using Fluorescent Fiber-Optic Confocal Microscopic Imaging, J. Invest. Dermatol. 121 (2003) 706–712, https://doi.org/10.1046/J.1523-1747.2003.12477.X.
[50] A. Dabbagh, R.A. Mahmoodian, B.J.J. Abdullah, H. Abdullah, M. Hamdi, N.H. Abu Kasim, Low-melting-point polymeric nanoshells for thermal-triggered drug release under hyperthermia condition, International Journal of Hyperthermia 31 (2015) 920–929, https://doi.org/10.3109/02656736.2015.1094147.
[51] K. Shameli, M. Bin Ahmad, S.D. Jazayeri, S. Sedaghat, P. Shabanzadeh, H. Jahangirian, M. Mahdavi, Y. Abdollahi, Synthesis and Characterization of Polyethylene Glycol Mediated Silver Nanoparticles by the Green Method, Int. J. Mol. Sci. 13 (2012) 6639–6650, https://doi.org/10.3390/IJMS13066639.